Journal of Power Sources 187 (2009) 8–18

Contents lists available at ScienceDirect

Journal of Power Sources

journal homepage: www.elsevier.com/locate/jpowsour

Numerical analysis of electrical power generation and internal reforming characteristics in seal-less disk-type solid oxide fuel cells

Takanobu Shimada [a,*], Akihiko Momma [b], Kiyonami Takano [b], Tohru Kato [b]

[a] Department of Electrical Engineering, Graduate School of Science and Technology, Tokyo University of Science, 2641 Yamazaki, Noda, Chiba 278-8510, Japan
[b] Fuel Cell System Group, Energy Technology Research Institute, National Institute of Advanced Industrial Science and Technology (AIST), Tsukuba Central 2, 1-1-1 Umezono, Tsukuba, Ibaraki 305-8568, Japan

ARTICLE INFO

Article history:
Received 4 September 2008
Received in revised form 22 October 2008
Accepted 24 October 2008
Available online 8 November 2008

Keywords:
Solid oxide fuel cell
Simulation
Internal reforming
Diffusion
Seal-less
Concentration profile

ABSTRACT

For seal-less type solid oxide fuel cells, its power generation characteristics and distribution of the gas composition depend on not only the electrochemical reaction, but also complex kinetics and transport phenomena, because the internal reforming reaction and the water-gas shift reaction take place together with reverse diffusion of the ambient gas from the surroundings of the cell. The purpose of this paper is to theoretically explain the experimental results of the anodic concentration profile of gaseous species previously reported in a practical seal-less disk-type cell which used pre-reforming methane with steam as a fuel. A numerical model that takes into account the transport phenomena of the gaseous species and the internal reforming reaction with the water-gas shift reaction together with the assumption of the cell outlet boundary condition was constructed to numerically analyse the gas composition distribution and power generation characteristics. Numerical analyses by the model were conducted for the several cases reported as the experiment. The calculated results in the anode gas concentration profile and in the voltage–current characteristics show good agreement with the experimental data in every case, and then the validity of the simulation model was verified. Therefore, the model is useful for a seal-less disk-type cell which is operated by a fuel including non-reformed methane.

© 2008 Elsevier B.V. All rights reserved.

1. Introduction

Solid oxide fuel cells (SOFCs) have attracted much attention due to their high efficiency and cleanliness, and they are expected to be one of the most favorable electrical power generation technologies in the near future. Recently, SOFC systems driven by town gas have been intensively developed by several companies using seal-less cell structure, where the outlet edges of the gas channels of the anode and cathode are open to the ambient, owing to its advantageous features in gas sealing and thermal stress problems [1–3].

In the SOFC systems, an internal reforming, i.e., reforming of the fuel in the cell, is often employed in conjunction with pre-reforming due to its high operating temperature. Generally, the power generation characteristics of cells depend on the gas composition on the anode side and cathode side of the cells. In the seal-less type cells, the internal reforming reaction and the water-gas shift reaction take place together with reverse diffusion of the ambient gas from the surroundings of the cell, i.e., diffusion opposite to gas flow direction. Therefore, the distribution of the gas composition in the cell and power generation characteristics depends on not only the electrochemical reaction, but also complex kinetics. Many simulation studies have been conducted to aid in development of SOFCs [4–19].

To the best of our knowledge, however, very few numerical results have been reported on the power generation characteristics compared to the measurement of the gas composition distributions because the concentration profile of the gaseous species in a cell has been seldom measured. For the seal-less disk-type cell using pure hydrogen as a fuel, it has been reported by Momma et al. [17] that the influence of the reverse diffusion of the ambient gas is clarified based on both the experimental and theoretical analyses, the results of which have shown good agreement. On the other hand, there has never been such practicably useful report on the cell using reformed gas as the fuel.

In one of the recent papers dealing with seal-less disk-type SOFCs, Momma et al. [20], reported the experimental results for the concentration profile of gaseous species along the flow direction in the anode gas channel of the single cells which were performed

* Corresponding author at: Space Power Systems Group, Institute of Space and Aeronautical Science (ISAS), Japan Aerospace Exploration Agency (JAXA), 3-1-1 Yoshinodai, Sagamihara, Kanagawa 229-8510, Japan. Tel.: +81 427 59 8688; fax: +81 42 59 8068.
E-mail address: shimada.takanobu@jaxa.jp (T. Shimada).

0378-7753/$ – see front matter © 2008 Elsevier B.V. All rights reserved.
doi:10.1016/j.jpowsour.2008.10.125

Nomenclature

c	molar density (mol m^{-3})
c_{CO}	CO concentration in the mixture gas (mol m^{-3})
c_{H_2O}	H_2O concentration in the mixture gas (mol m^{-3})
$\dot{c}_j$	mole reaction quantity due to cell reaction for each unit time and unit volume (mol s^{-1} m^{-3})
$\dot{c}_{ref}$	mole reaction quantity due to reforming reaction for each unit time and unit volume (mol s^{-1} m^{-3})
$\dot{c}_{sf}$	mole reaction quantity due to water-gas shift reaction for each unit time and unit volume (mol s^{-1} m^{-3})
D_{AB}	mutual diffusion coefficient of species A and B (m^2 s^{-1})
d_{an}	thickness of anode current collector
d_{ca}	thickness of cathode current collector
D_e	effective diffusion coefficient (m^2 s^{-1})
$D_{i,m}$	diffusion coefficient of species i in multi-component mixture gas (m^2 s^{-1})
D_{1j}	diffusion coefficient of the pair of 1–j species in a binary mixture (m^2 s^{-1})
D_{1m}	diffusion coefficient when element 1 diffuses in the mixture gas m
Ea_r	activation energy (J mol^{-1})
ΔEa_{ref}	activation energy (=57,840 J mol^{-1})
ΔEa_{sf}	activation energy (=95,000 J mol^{-1})
$\Delta G^{\circ}_{H_2O}$	Gibbs free energy change in reaction $H_2 + O_2 = H_2O$ at the standard pressure (0.1 MPa) and reference state (J mol^{-1})
F	Faraday constant (C mol^{-1})
J_e	electronic current density which flows in electrolyte (A m^{-2})
J_i	ionic current density which flows in electrolyte (A m^{-2})
J_o	current density which flows to an external circuit (A m^{-2})
k	Boltzmann constant (=1.3807 × 10^{-23} J K^{-1})
K_{sf}	equilibrium constant of water-gas shift reaction
M_i	molecular weight of species i (kg mol^{-1})
P	pressure (Pa)
p_{CH_4}	partial pressure of methane in the mixture gas
p_i	partial pressure of chemical species i
R	gas constant (=8.314 J mol^{-1} K^{-1})
r_{cell}	radius of the cell
R_{cell}	cell resistance (Ω m^2)
R_{cell_0}	cell resistance at 1073 K (Ω m^2)
R_e	ohmic resistance of electrolyte by electronic conduction (Ω m^2)
R_i	ohmic resistance of electrolyte by ionic conduction (Ω m^2)
R_r	reactive resistance of the electrodes (Ω m^2)
R_s	series resistance of the electrodes (Ω m^2)
r_{CH_4}	rate of the reforming reaction (mol s^{-1} kg$^{-1}_{cat}$)
r_{CO}	rate of the water-gas shift reaction (mol s^{-1} kg$^{-1}_{cat}$)
T	temperature (K)
T_{cell}	temperature of the cell
T_{ref}	outlet gas temperature of pre-reformer (K)
V_{cell}	cell operating voltage (V)
u	mass average velocity (m s^{-1})
U_f	fuel utilization

Greek letters

α_{ref}	utilization factor by which the catalyst in the anode current collector actually contributes to the reforming reaction
α_{sf}	utilization factor by which the catalyst in the anode current collector actually contributes to the water-gas shift reaction
ε_{an}	porosity of the anode current collector
ε_{ca}	porosity of the cathode current collector
ε_{po}	porosity
σ	characteristic diameter (Å)
ρ	total mass density (kg m^{-3})
ρ_{anc}	density of anode current collector (kg m^{-3})
$\rho_{cat,ref}$	density of catalysts which actually contribute to the reforming reactions (kg m^{-3})
$\rho_{cat,sf}$	density of catalysts which actually contribute to the water-gas shift reactions (kg m^{-3})
τ	twist factor
χ	molar fraction
Ω	collision integration
ω_i	mass fraction of species i

Subscripts

an	fuel (anode gas)
ca	air (cathode gas).

by partially reformed methane as the fuel. From the compositional analysis of the anode gas, their experimental results indicated that the molar ratio of the hydrogen and carbon elements, i.e., H/C, is not a constant value between the inlet and outlet of the anode gas channel, and that nitrogen, which is not surely present in the inlet, is significantly detected near the cell edge. The following conclusions are suggested: (1) there are different diffusion velocities, or different species velocities, between each chemical species that composes the anode gases, and (2) reverse diffusion of ambient air from the periphery of the cell takes place.

In this paper, to theoretically clarify these phenomena, a numerical model that takes the convection of the gas and diffusion into account was constructed for a seal-less disk-type SOFC which is operated by a fuel including non-reformed methane. Therefore, we compared the numerical results with the experimental data such as the concentration distributions of the gaseous species and voltage–current characteristics using the calculation corresponding to the experimental conditions, and then examined these phenomena. This model can explain the influence of an internal reforming reaction and a water-gas shift reaction in the anode gas flow together with the reverse diffusion from the periphery of the cell. Furthermore, this model suggests the distributions of an electromotive force and a current because it deals with the distributions of the concentration profile of gaseous species along the flow direction, thereby the voltage–current characteristics are predicted.

2. Modeling

2.1. Simulation model and assumption

Fig. 1 shows a schematic diagram of a seal-less disk-type SOFC single cell as a simulation model used to explain the data obtained from the experiment of Momma et al. [20]. The model consists of a composite disk made of a solid electrolyte with electrodes on both sides, and current collectors and metal separators, each for the positive and negative electrodes.

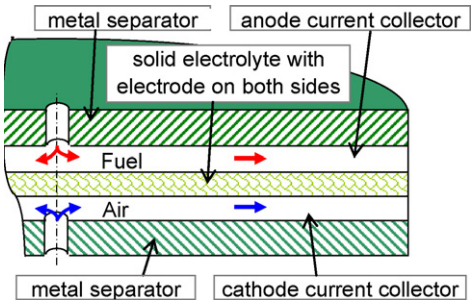

Fig. 1. A schematic diagram of the seal-less disk-type SOFC single cell.

The fuel, which consists of equilibrium compositions determined by the pre-reformer temperature, is first supplied to the anode gas channel (current collector) through orifices located at the center of the separator. The fuel is then axial symmetrically distributed in the current collectors (Fig. 1). The air is also supplied and distributed in the cathode gas channel in the same manner as the fuel. The remaining fuel after the fuel cell reaction is burned around the cell.

The following describes the prerequisites and assumptions of the model:

1. The gases have one-dimensional axisymmetric flows.
2. The cell temperature is constant along with the thickness and radius direction.
3. The inner pressure of the cell is constant.
4. The height of the gas channel (the current collectors) is constant.
5. The structure of the cell is constant throughout the cell.
6. The composition of gases consists of CH_4, H_2O, H_2, CO, CO_2 and N_2 in the anode, while of O_2 and N_2 in the cathode.
7. The concentration of each gas species is constant in the direction of gas channel thickness.
8. As an inlet boundary condition, at the center of the disk-type cell, the composition of each chemical species in the anode gas is in equilibrium as determined by the outlet gas temperature of the pre-reformer.
9. As an outlet boundary condition, at the periphery of the disk-type cell, the air exists as a stoichiometric amount for burning all the CH_4, H_2, and CO in the anode gas. In other words, the partial pressures of CH_4, H_2 and CO are zero, and N_2 exists 0.79/0.21 times as much as O_2 used to stoichiometrically burn the fuel at the periphery of the cell.

For items 1–5, it is ideally presumed to simplify the cell model simulating the experiment. As for item 1, the previous experimental result by Momma et al. [17] significantly demonstrated that the gaseous flow has no substantial variations along the circumferential direction in the practical seal-less disk-type cells using only hydrogen, steam and nitrogen as the anode gases. As for item 6, oxygen in the anode gas can be ignored on the basis of the experiment. Item 7 is an assumption for the one-dimensional calculation, meaning that the mixing velocity in the direction of the thickness is much faster than the velocity of the radial convection. However, there is no validity near the inlet, and this point will be discussed later. The basis of item 8 is a result of the experiment [20]. Although item 9 is a bold assumption for simplification, it is confirmed to be appropriate, because the simulation result and experimental result well agree as will be shown later.

In the anode current collector, the fuel containing residual methane and carbon monoxide is reformed by internal reforming reactions.

Table 1
Description of the anode current collectors used in the experiments.

Type	Material	Thickness [mm]	Mass [g m^{-2}]	Density [kg m^{-3}]
Type-A	Ni-foam	0.62	440	709
Type-C	Ni-SDC impregnated Ni-foam/Ni-foam	1.0	1600	1600

Reforming reaction : $CH_4 + H_2O \rightarrow 3H_2 + CO$ (1)

Water-gas shift reaction : $CO + H_2O \rightarrow H_2 + CO_2$ (2)

The reaction rates for the reforming reaction and water-gas shift reaction are assumed in Eqs. (3) and (4), respectively.

$$r_{CH_4} = 1.76 \times 10^3 \exp\left(\frac{-\Delta Ea_{ref}}{RT}\right)(p_{CH_4})^{1.2} \quad (3)$$

where r_{CH_4} is the rate of the reforming reaction [mol s^{-1} kg$_{cat}^{-1}$], ΔEa_{ref} is the activation energy (=57,840 J mol^{-1}), R is the gas constant (=8.314 J mol^{-1} K^{-1}), T is the temperature [K], and p_{CH_4} is the partial pressure of methane in the mixture gas [atm] [21]. The reason why Eq. (3) is chosen as the reaction rates for the reforming reaction is that it offers a good fit to the experimental gas concentration distributions as compared with the expression reported by Lee et al. [22].

$$r_{CO} = 26.1 \times 10^3 \exp\left(\frac{-\Delta Ea_{sf}}{RT}\right)(c_{CO})^{1.1}(c_{H_2O})^{0.53}(1-\beta) \quad (4)$$

$$\beta = \frac{p_{CO_2} p_{H_2}}{K_{sf} p_{CO} p_{H_2O}} \quad (5)$$

where r_{CO} is the rate of the water-gas shift reaction [mol s^{-1} kg$_{cat}^{-1}$], ΔEa_{sf} is the activation energy (=95,000 J mol^{-1}), c_{CO} is the CO concentration in the mixture gas [mol m^{-3}], c_{H_2O} is the H_2O concentration in the mixture gas [mol m^{-3}], K_{sf} is the equilibrium constant of Eq. (2), and p_i is the partial pressure of the chemical species i [23]. Therefore, the molar reaction quantity per each unit time and unit volume in Eqs. (3) and (4) [mol s^{-1} m^{-3}], $\dot{c}_{ref}$ and $\dot{c}_{sf}$, are obtained from,

$$\dot{c}_{ref} = r_{CH_4}\, \rho_{cat,ref} \quad (6)$$

$$\dot{c}_{sf} = r_{CO}\, \rho_{cat,sf} \quad (7)$$

where $\rho_{cat,ref}$ and $\rho_{cat,sf}$ are the density of the catalysts, respectively which actually contribute to the reforming and water-gas shift reactions [kg m^{-3}], and are stated as follows:

$$\rho_{cat,ref} = \rho_{anc}\, \alpha_{ref} \quad (8)$$

$$\rho_{cat,sf} = \rho_{anc}\, \alpha_{sf} \quad (9)$$

where ρ_{anc} is the density of the anode current collector (see Table 1) [kg m^{-3}], and α_{ref} and α_{sf} are defined here as the utilizations of the catalyst in percentages by which the catalyst in the anode current collector actually contributes to the above reactions. These values are experimentally determined as shown in Section 3.1.1.

On the other hand, the concentrations of the chemical species in the fuel and air change based on the electrochemical cell reactions in Eq. (10)

$$\begin{aligned} H_2 + O^{2-} &\rightarrow H_2O + 2e^- \quad \text{at anode} \\ \tfrac{1}{2}O_2 + 2e^- &\rightarrow O^{2-} \quad \text{at cathode} \end{aligned} \quad (10)$$

It is assumed here that CO is consumed only in the shift reaction and not by the direct electrochemical reaction of CO. The local electromotive force E_{emf} is obtained by the Nernst equation from the O_2

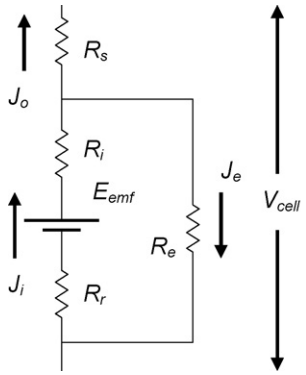

Fig. 2. Equivalent circuit of the disk-type cell.

partial pressure ratio of the anode and cathode assuming that H_2, O_2 and H_2O in the anode gas are in thermal equilibrium.

$$E_{emf} = -\frac{\Delta G^{\circ}_{H_2O}}{2F} + \frac{RT}{2F}\ln\frac{p_{H_2}\,p_{O_2}^{0.5}}{p_{H_2O}} \tag{11}$$

where $\Delta G^{\circ}_{H_2O}$ is the Gibbs free energy ($H_2 + O_2 = H_2O$), and F is Faraday constant.

The equivalent circuit of the disk-type cell assumed as the model is shown in Fig. 2 [17], which stands for a local circuit segmented from the whole SOFC. Each symbol in Fig. 2 denotes as follows: R_i, ohmic resistance of the electrolyte by ionic conduction [Ωcm^2]; R_e, ohmic resistance of electrolyte by electronic conduction [Ωm^2]; R_r, reactive resistance of the electrodes [Ωm^2]; R_s, series resistance of the electrodes [Ωcm^2]; J_i, ionic current density which flows in the electrolyte [A m^{-2}]; J_e, electronic current density which flows in the electrolyte [A m^{-2}]; J_o, current density which flows in an external circuit [A m^{-2}]; and V_{cell}, cell operating voltage [V]. These cell resistances are assumed to be a function of the temperature, and are given by

$$R_{cell} = R_{cell_0}\exp\left[\frac{Ea_r}{R}\left(\frac{1}{T} - \frac{1}{1073}\right)\right] \tag{12}$$

where R_{cell} means each resistances described above in [Ωm^2], R_{cell0} is the resistance at 1073 K [Ωm^2], and Ea_r is the activation energy [J mol^{-1}] (see Table 2) [8]. These values were experimentally determined by an AC impedance measurement of the cell. The whole cell current is written as

$$I_{cell} = \int_0^{r_{cell}} J_o 2\pi r\,\mathrm{d}r \tag{13}$$

where J_o means the local current density and is obtained from

$$J_o = \frac{E_{emf}R_e - V_{cell}(R_i + R_r + R_e)}{R_e(R_i + R_r + R_s) + R_s(R_i + R_r)}. \tag{14}$$

The molar reaction rate in the anode and cathode by the cell reaction for each unit time and unit volume [mol s^{-1} m^{-3}], $\dot{c}_j$ and $\dot{c}'_j$, is obtained from, respectively

$$\dot{c}_j = \frac{J_o + J_e}{2F}\frac{1}{d_{an}} = \frac{J_i}{2F}\frac{1}{d_{an}} \tag{15}$$

$$\dot{c}'_j = \frac{J_o + J_e}{2F}\frac{1}{d_{ca}} = \frac{J_i}{2F}\frac{1}{d_{ca}} \tag{16}$$

where d_{an} is the thickness of the anode current collector (see Table 2) and d_{ca} is the thickness of the cathode current collector.

Table 2
Simulation parameters.

Cell size		
Radius of the cell	r_{cell}	6 cm
Thickness of the anode current collector	d_{an}	See Table 1
Porosity of the anode current collector	ε_{an}	0.95
Thickness of the cathode current collector	d_{ca}	0.07 cm
Porosity of the cathode current collector	ε_{ca}	0.95
Physical properties of cell		
Density of the anode current collector	ρ_{an}	See Table 1
Twist factor of the anode current collector	τ_{an}	1
Twist factor of the cathode current collector	τ_{ca}	1
Ohmic resistance of electrolyte by ionic conduction at 800 °C	R_{i0}	0.17 Ω cm^2
Activation energy of R_i	Ea_i	54,200 J mol^{-1}
Ohmic resistance of electrolyte by electron conduction at 800 °C	R_{e0}	20 Ω cm^2
Activation energy of R_e	Ea_e	54,200 J mol^{-1}
Reactive resistance of the electrodes at 800 °C	R_{r0}	0.04 Ω cm^2
Activation energy of R_r	Ea_r	50,200 J mol^{-1}
Series resistance of the electrodes at 800 °C	R_{s0}	0.002 Ω cm^2
Activation energy of R_s	Ea_s	54,200 J mol^{-1}
Operating conditions		
Flow rate of the fuel (methane)		85 Ncc min^{-1}
Flow rate of the air		1700 Ncc min^{-1}
Oxygen fraction in the air		0.21
Inner pressure of the cell	P	1 atm
Room temperature	T_{room}	25 °C
Outlet gas temperature of pre-reformer	T_{ref}	650, 600, 550 °C
Temperature of the cell	T_{cell}	750 °C
Fuel utilization	U_f	0, 50, 70%
Steam–carbon ratio	S/C	3.0

2.2. Transport equation of gas flow

The concentration distribution of each gaseous species, cell voltage and cell current density are calculated in such a way that the equations of mass balance and the equation of continuity are converted into discrete equations by the control-volume method using the implicit method and upwind scheme.

2.2.1. Equation of mass balance for each species

Anode side:

$$\mathrm{CH_4}: \quad \frac{\partial}{r\partial r}\left(r\rho_{an}\omega_{CH_4}u_{an} - rD_{CH_4,m}\rho_{an}\frac{\partial\omega_{CH_4}}{\partial r}\right) = \left(-\dot{c}_{ref}\right)M_{CH_4} \tag{17}$$

$$\mathrm{H_2O}: \quad \frac{\partial}{r\partial r}\left(r\rho_{an}\omega_{H_2O}u_{an} - rD_{H_2O,m}\rho_{an}\frac{\partial\omega_{H_2O}}{\partial r}\right) = \left(-\dot{c}_{ref} - \dot{c}_{sf} + \dot{c}_j\right)M_{H_2O} \tag{18}$$

$$\mathrm{H_2}: \quad \frac{\partial}{r\partial r}\left(r\rho_{an}\omega_{H_2}u_{an} - rD_{H_2,m}\rho_{an}\frac{\partial\omega_{H_2}}{\partial r}\right) = \left(3\dot{c}_{ref} + \dot{c}_{sf} - \dot{c}_j\right)M_{H_2} \tag{19}$$

$$\mathrm{CO}: \quad \frac{\partial}{r\partial r}\left(r\rho_{an}\omega_{CO}u_{an} - rD_{CO,m}\rho_{an}\frac{\partial\omega_{CO}}{\partial r}\right) = \left(\dot{c}_{ref} - \dot{c}_{sf}\right)M_{CO} \tag{20}$$

$$CO_2: \quad \frac{\partial}{r\partial r}\left(r\rho_{an}\omega_{CO_2}u_{an} - rD_{CO_2,m}\rho_{an}\frac{\partial\omega_{CO_2}}{\partial r}\right) = \left(\dot{c}_{sf}\right)M_{CO_2} \tag{21}$$

$$N_{2an}: \quad \frac{\partial}{r\partial r}\left(r\rho_{an}\omega_{N_{2an}}u_{an} - rD_{N_{2an},m}\rho_{an}\frac{\partial\omega_{N_{2an}}}{\partial r}\right) = 0 \tag{22}$$

Cathode side:

$$O_2: \quad \frac{\partial}{r\partial r}\left(r\rho_{ca}\omega_{O_2}u_{ca} - rD_{O_2N_2}\rho_{ca}\frac{\partial\omega_{O_2}}{\partial r}\right) = \left(-0.5\dot{c}_j'\right)M_{O_2} \tag{23}$$

$$N_{2ca}: \quad \frac{\partial}{r\partial r}\left(r\rho_{ca}\omega_{N_2ca}u_{ca} - rD_{N_2O_2}\rho_{ca}\frac{\partial\omega_{N_2ca}}{\partial r}\right) = 0 \tag{24}$$

where ρ is the total mass density [kg m^{-3}], ω_i is the mass fraction of species i [−], u is the mass average velocity [m s^{-1}], $D_{i,m}$ is the diffusion coefficient of species i in the multi-component mixture gas [m^2 s^{-1}], M_i is the molecular weight of species i [kg mol^{-1}], suffix *an* means the fuel (anode gas) and suffix *ca* the air (cathode gas).

2.2.2. Equation of continuity

The equation of mass continuity is as follows. Derivation of the expression is described in Appendix A:

$$\frac{\partial\rho_{an}}{\partial t} + \frac{\partial}{r\partial r}(r\rho_{an}u_{an}) = \left(\frac{1}{2}\dot{c}_j\right)M_{O_2} \quad \text{at anode} \tag{25}$$

$$\frac{\partial\rho_{ca}}{\partial t} + \frac{\partial}{r\partial r}(r\rho_{ca}u_{ca}) = \left(-\frac{1}{2}\dot{c}_j'\right)M_{O_2} \quad \text{at cathode} \tag{26}$$

The mass density of the fuel and air is given by

$$\rho_{an} = \sum_i c_{an}\chi_i M_i \tag{27}$$

$$\rho_{ca} = \sum_j c_{ca}\chi_j M_j \tag{28}$$

where χ is the molar fraction [−], and the molar density [mol m^{-3}], c, is a value dependent only on the temperature T and pressure P, which are assumed to be constant in the cell.

$$c_{an} = c_{ca} = \frac{P}{RT} \tag{29}$$

2.2.3. Diffusion coefficient

The diffusion coefficients of a chemical species in the anode and cathode used in Eqs. (17)–(24) are calculated from the prediction value in a multi-component gas compound [24].

$$\frac{1-x_l}{D_{1m}} = \sum_{j=2}^{n}\frac{x_j}{D_{1j}} \tag{30}$$

where D_{1m} is the diffusion coefficient when element 1 diffuses in a mixture gas m, and D_{1j} is the diffusion coefficient of the pair 1–j of species in a binary mixture.

The diffusion coefficient of a binary mixture gas composed of A and B at low (normal) pressure is calculated by the following expressions:

$$D_{AB} = 1.858\times10^{-3}T^{3/2}\frac{[(M_A+M_B)/M_AM_B]^{1/2}}{P\sigma_{AB}^2\Omega_D} \tag{31}$$

$$\sigma_{AB} = \frac{\sigma_A+\sigma_B}{2} \tag{32}$$

$$\Omega_D = \frac{A}{T^{*B}} + \frac{C}{\exp(DT^*)} + \frac{E}{\exp(FT^*)} + \frac{G}{\exp(HT^*)} \tag{33}$$

where D_{AB} is the mutual diffusion coefficient of species A and B [m^2 s^{-1}], M_A and M_B are the molecular weights of species A and B [g mol^{-1}], respectively, P is the pressure [atm], σ_A and σ_B are the characteristic diameters of species A and B [Å], respectively, Ω_D is the collision integration, $T^* = kT/\varepsilon_{AB}$, $\varepsilon_{AB} = (\varepsilon_A\varepsilon_B)^{1/2}$, $A = 1.06036$, $B = 0.15610$, $C = 0.19300$, $D = 0.47635$, $E = 1.03587$, $F = 1.52996$, $G = 1.76474$, $H = 3.89411$, ε/k is the intermolecular force constant [K] and k is Boltzmann constant ($=1.3807\times10^{-23}$ J K^{-1}) [25].

An effective diffusion coefficient, D_e, in porous current collectors is calculated as follows:

$$D_e = \frac{\varepsilon_{po}}{\tau}D_{AB} \tag{34}$$

where τ is the twist factor [−] and ε_{po} is the porosity [−] [26]. In this paper, the equations of mass balance shown in Eqs. (17)–(24) are calculated by taking the effective diffusion coefficient into consideration.

2.3. Analytical conditions

In the experiment by Momma et al., three types of current collectors with different structures and materials, which also serve as the channel for the fuel gas, were tested for comparison of the internal reforming characteristics [20]. However, only two types of the current collectors having significantly different reforming characteristic, type-A and type-C (see Table 1), are discussed in this paper because the reforming characteristic of the current collector type-A was similar to that of type-B. Measurements were made by varying the fuel utilization ($U_f = 0$, 50, 70%) at various pre-reformer exit temperatures ($T_{ref} = 550$, 600, 650 °C) with a steam to carbon ratio of S/C = 3.0 at the cell temperature of 750 °C.

The physical property values and the operating conditions used in the calculations are indicated in Table 2. The simulation parameters, such as cell sizes and physical properties and operating conditions, are adjusted to the experimental conditions as shown in reference [20].

3. Results and discussion

3.1. Anode current collector type-C

3.1.1. Decision on parameters of the reaction rate by comparison with experimental results

As for the reaction rates of the reforming reaction and water-gas shift reaction, the percentages that the catalyst (Ni) actually works for the reactions are treated as the unknown parameters, α_{ref} and α_{sf}. The optimum values to fit the calculated gas concentration profile to the experimental ones are found by varying α_{ref} and α_{sf} at only one condition of $T_{ref} = 550$ °C and $U_f = 70\%$. The reason why $T_{ref} = 550$ °C is chosen is that more non-reformed methane is contained in the fuel cell due to the reforming temperature lower than 650 and 600 °C. Also, the reason why $U_f = 70\%$ is chosen is that the greatest variation in each chemical species concentration is observed between the center and the periphery of the cell due to the most progressive electrochemical reactions. Therefore, it is an advantage to confirm the effect of the selected parameters on the gas concentration distributions when the numerical results are compared to the experimental data. The parameters for the percentage and the densities corresponding to it are listed in Table 3. The value, α_{ref}, is assumed to be equal to α_{sf} for simplification of the calculation.

The gas concentration distributions of CH_4, H_2O, H_2, CO and CO_2 for each condition in Table 3 are shown in Figs. 3–7. The experimental values at the radii of 0, 1.4, 2.8, 4.2 and 5.6 cm are jointly

Table 3
Conditions for a decision on the reaction rate parameters.

	Cond.1	Cond.2	Cond.3	Cond.4
α_{ref}, α_{sf} [−]	0.05	0.04	0.03	0.02
ρ_{ref}, ρ_{sf} [kg m^{-3}]	80	64	48	32

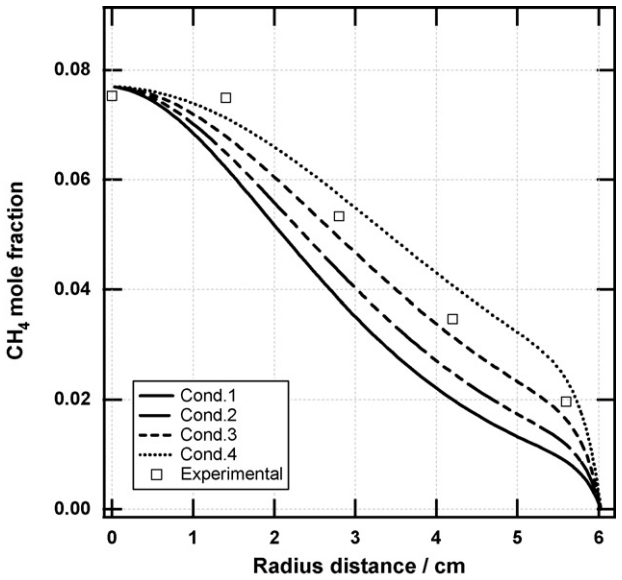

Fig. 3. CH_4 distributions for each condition and experimental data (T_{ref} = 550 °C, U_f = 70%, type-C).

plotted on the figures. It can be seen from these figures that the experimental values are the closest to the calculation results for condition 3, i.e., $\alpha_{ref} = \alpha_{sf} = 0.03$, or $\rho_{ref} = \rho_{sf} = 48\ \mathrm{kg\,m^{-3}}$. Therefore, the density of the catalysts, which actually contribute to the reforming and water-gas shift reactions is set at 48 kg m^{-3} for the anode current collector type-C. Using this value, the gas concentration distributions are likewise calculated for the other conditions, and the validity of the parameter is evaluated in the following section.

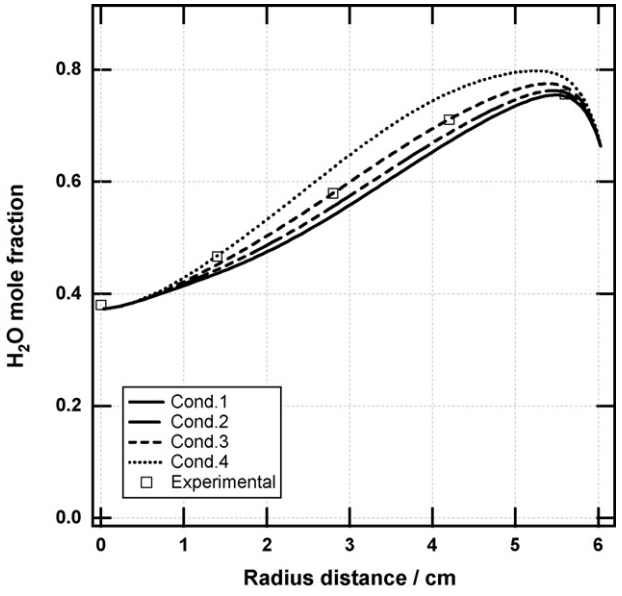

Fig. 4. H_2O distributions for each condition and experimental data (T_{ref} = 550 °C, U_f = 70%, type-C).

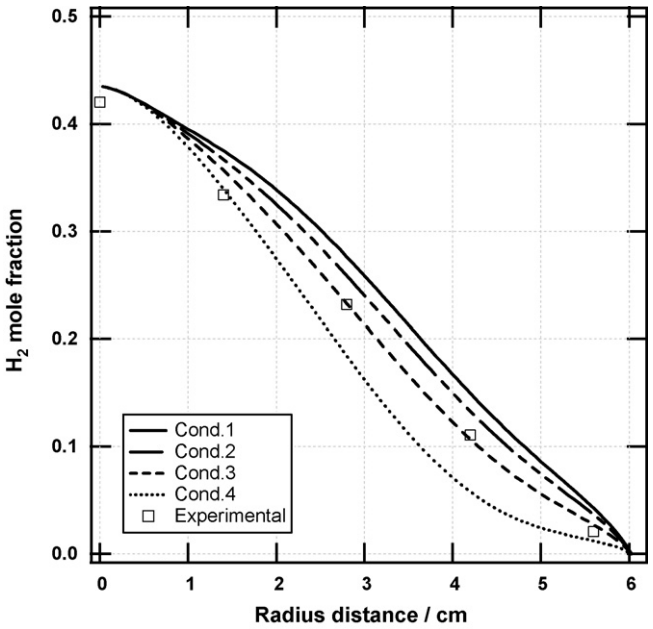

Fig. 5. H_2 distributions for each condition and experimental data (T_{ref} = 550 °C, U_f = 70%, type-C).

As a further consideration, from Fig. 3, the experimental CH_4 concentration hardly changes between r = 0 cm and r = 1.4 cm unlike the calculated result, and the experimental H_2O concentration at 1.4 cm is higher than the calculated one, while the experimental H_2 and CO concentrations are lower than the simultaneously calculated values (see Figs. 4–6). It is interpreted that there is no reforming reaction in this region. That is, the region where the catalyst effectively performs becomes small because the diffusion of the gas in the thickness direction is lower than the radial convective flow due to the higher velocity near the center. On the other hand, in this model, the diffusion in the thickness direction is assumed to be sufficiently greater than the radial convection. In other words,

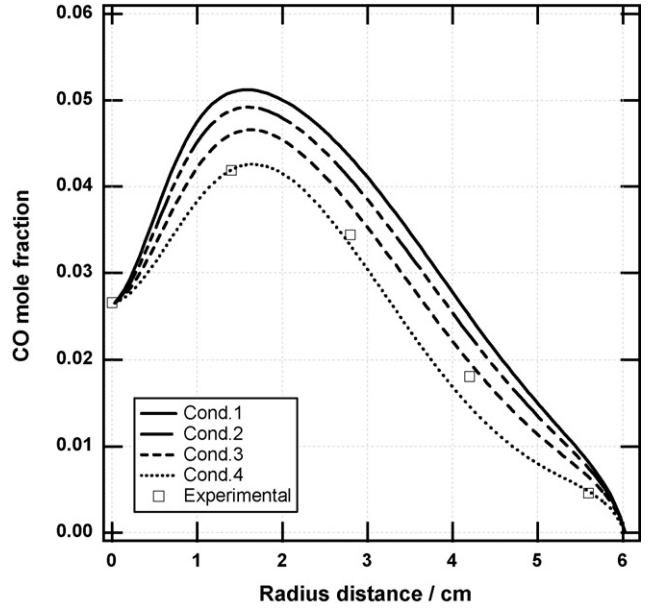

Fig. 6. CO distributions for each condition and experimental data (T_{ref} = 550 °C, U_f = 70%, type-C).

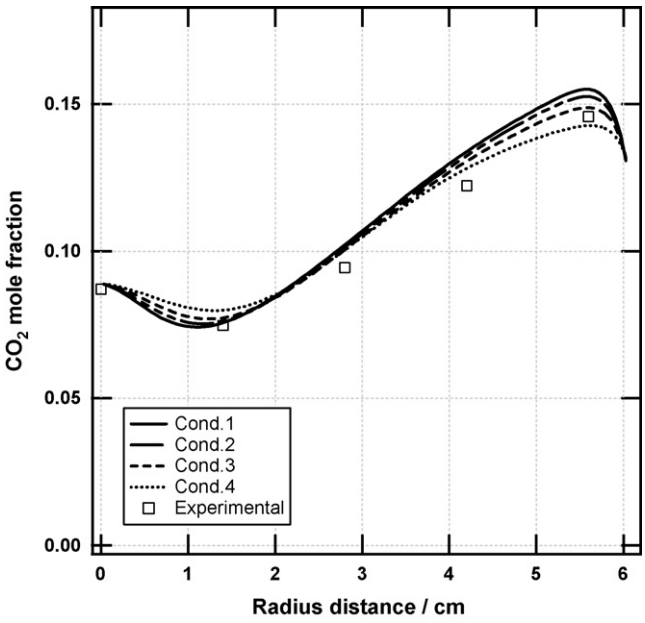

Fig. 7. CO_2 distributions for each condition and experimental data (T_{ref} = 550 °C, U_f = 70%, type-C).

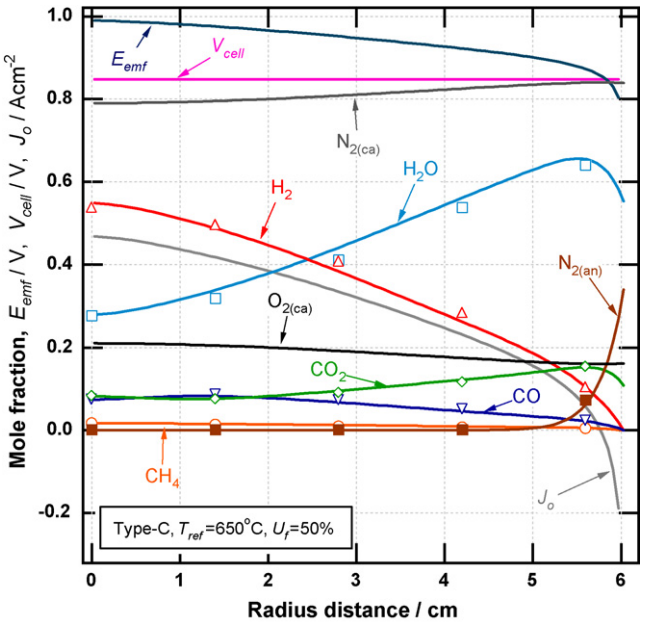

Fig. 9. Distributions of gas concentration, electromotive force, cell voltage, and current density (T_{ref} = 650 °C, U_f = 50%, type-C).

the assumption that the distribution of the gas concentration in the thickness direction is not considered is not suitable in the near inlet.

However, the entire tendency of the numerical results is in good agreement with the experimental values although the distribution is not in close agreement from r = 0 to r = 1.4 cm.

3.1.2. Gas concentration distributions in the cell at various pre-reformer temperatures and fuel utilization

Using the reaction rate parameter determined in the above investigation, the distributions of gas concentrations are calculated and then compared to the experimental results for each condition of the pre-reformer temperatures of 650, 600 and 550 °C and fuel utilizations of 0, 50 and 70%. Thereafter, the validity of the simulation model is examined. The distributions of each gas concentration, electromotive force, cell voltage and current density are displayed in Figs. 8–15. The result when T_{ref} = 550 °C and U_f = 50% is omitted because it was not measured. The experimental values at the radii of 0, 1.4, 2.8, 4.2 and 5.6 cm are jointly plotted on the figures indicated by the symbols of (○) CH_4, (□) H_2O, (△) H_2, (▽) CO, (◊) CO_2 and (■) N_2 in the anode.

The calculated concentration distributions of the anode gas species well agree with the experimental in every case for the pre-reformer temperatures and the fuel utilizations.

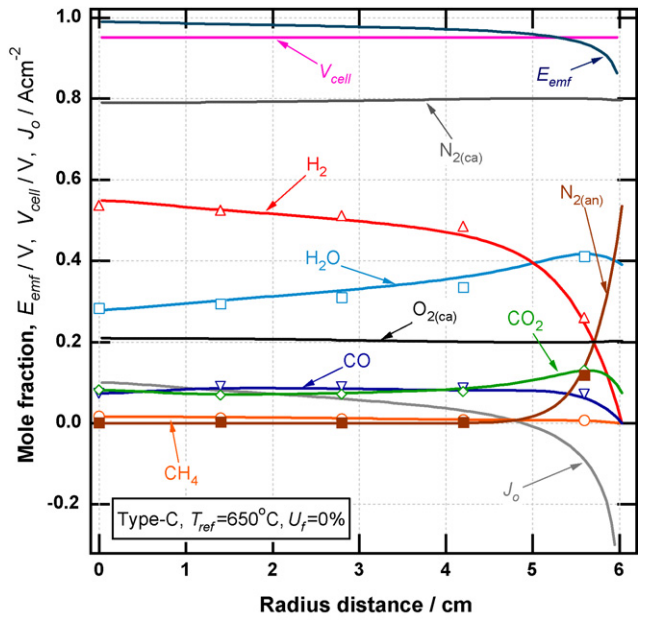

Fig. 8. Distributions of gas concentration, electromotive force, cell voltage, and current density (T_{ref} = 650 °C, U_f = 0%, type-C).

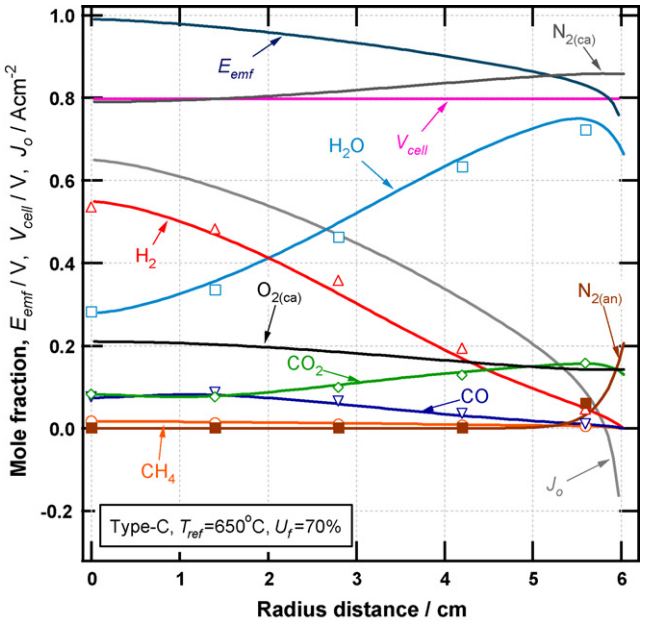

Fig. 10. Distributions of gas concentration, electromotive force, cell voltage, and current density (T_{ref} = 650 °C, U_f = 70%, type-C).

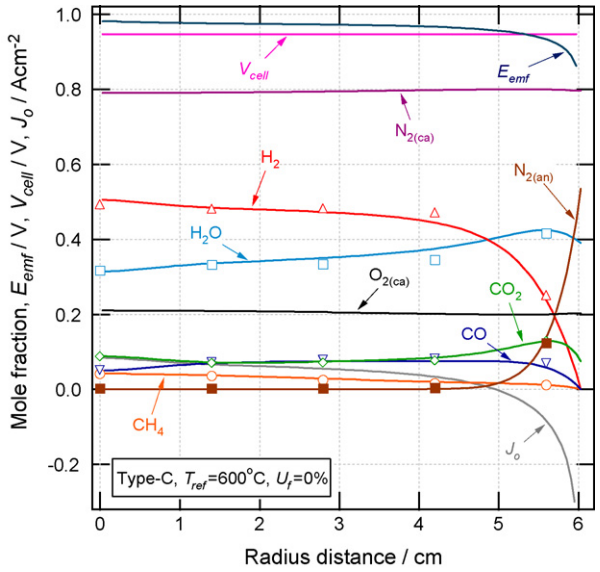

Fig. 11. Distributions of gas concentration, electromotive force, cell voltage, and current density (T_{ref} = 600 °C, U_f = 0%, type-C).

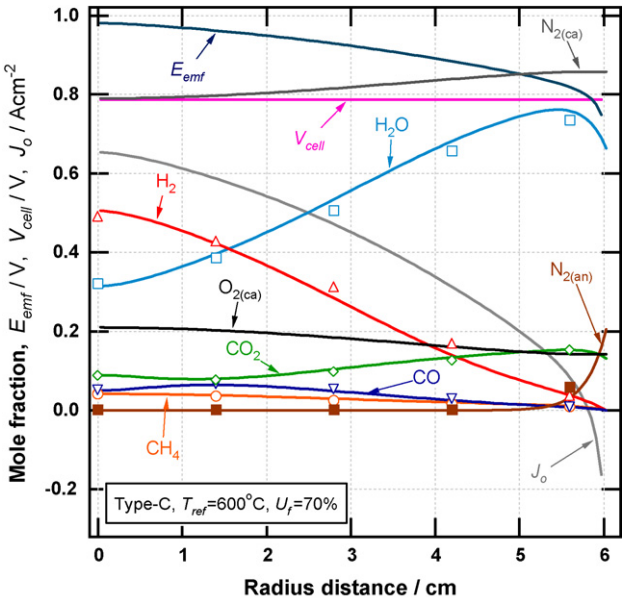

Fig. 13. Distributions of gas concentration, electromotive force, cell voltage, and current density (T_{ref} = 600 °C, U_f = 70%, type-C).

In the experiment, the distinct effect of internal reforming is observed for the anode current collector type-C. As shown in every figure, the experimental well agrees with the calculation results of the CH_4 concentration that decreases along the flow direction due to the reforming reaction. This good agreement suggests that the reforming reaction of the cell used in the experiment can be well described by the reaction rate equation (Eq. (3)).

For the CO and CO_2 concentration distributions, the considered model can describe the phenomenon that the CO concentration increases (CO_2 decreases), i.e., the reverse-shift reaction, from the center of the cell to around 1.4 cm in radius (2.8 cm in U_f = 0% due to a lower H_2O concentration), while the CO concentration decreases (CO_2 increases), i.e., the shift reaction, from its outside because the H_2O concentration increases and the H_2 concentration decreases due to the electrochemical reaction. Therefore, the reaction rate equation of the shift reaction can model the experimental result.

It can be confirmed from the calculation results that the N_2 concentration distributions observed in the anode gas channel in the experiment are due to the reverse diffusion from the periphery. It is noted from Figs. 8 to 15 that the reverse diffusion of N_2 takes place more remarkably as the fuel utilization U_f is lower; i.e., hydrogen exists more in the gas channel due to its lower consumption. This is because the diffusion coefficient in the anode gas mixture of nitrogen becomes high when the fraction of the hydrogen component in the gas increases. This is also further discussed in Section 3.1.3.

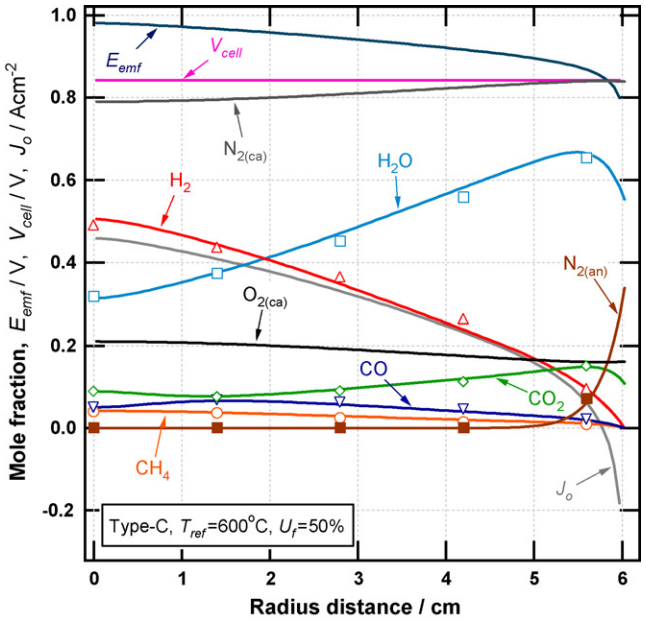

Fig. 12. Distributions of gas concentration, electromotive force, cell voltage, and current density (T_{ref} = 600 °C, U_f = 50%, type-C).

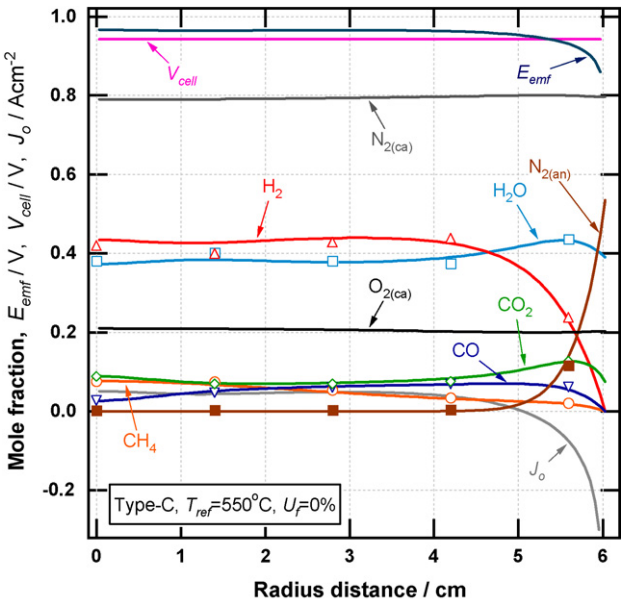

Fig. 14. Distributions of gas concentration, electromotive force, cell voltage, and current density (T_{ref} = 550 °C, U_f = 0%, type-C).

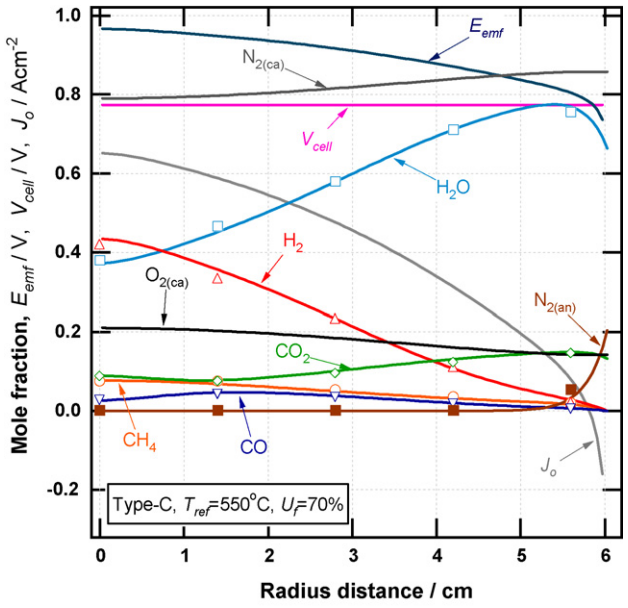

Fig. 15. Distributions of gas concentration, electromotive force, cell voltage, and current density (T_{ref} = 550 °C, U_f = 70%, type-C).

When U_f = 0%, the concentration of H_2 sharply decreases in the range r > 4.2 cm. This is caused by the decrease in the H_2 concentration at the outlet cell because H_2 is consumed by the oxidization with O_2 in the periphery of the cell, leading to an increased H_2 diffusion velocity by the concentration difference. The boundary condition at the cell outlet is assumed for H_2 to be completely consumed. The calculated H_2 and N_2 concentrations at r = 5.6 cm are in good agreement with the experimental data for each fuel utilization. Therefore, the assumption at the outlet boundary condition can describe the experiment results very well. As a consequence, as shown in Figs. 8–15 it is predicted that the electrolysis current is induced in the vicinity of the cell edge in which E_{emf} becomes less than V_{cell}.

Therefore, it is summarized that the reverse diffusion of air from the cell edge, the internal reforming reaction and the water-gas shift reaction can be well described, resulting in a good agreement between the calculated and experimental results for the concentration distributions of the anode gases.

3.1.3. Calculation of H/C mass balance, and comparison to experiment results

The carbon balance, $C_{balance}$, and hydrogen mass balance, $H_{balance}$, are still disputed. $C_{balance}$, and $H_{balance}$, are defined by Eq. (35) and Eq. (36), respectively.

$$C_{balance} = \chi_{CH_4} + \chi_{CO} + \chi_{CO_2} \quad (35)$$

$$H_{balance} = 4\chi_{CH_4} + 2\chi_{H_2} + 2\chi_{H_2O} \quad (36)$$

where χ_i denotes the molar fraction of gaseous species i.

In Fig. 16, the calculated $H_{balance}/C_{balance}$ is plotted together with the experimental values. The calculation results show a tendency similar to the experimental values versus the various parameters, such as r, T_{ref} and U_f. For the experimental values, while the observed $H_{balance}/C_{balance}$ remains approximately equal to its input value of 10 at $r \leqq 4.7$ cm, it suddenly decreases at r = 56 cm. Additionally, it decreases more with lower fuel utilization. This can be explained as follows. The low fuel utilization results in the significant existence of hydrogen which causes a high diffusion coefficient of hydrogen and high concentration gradient, $\partial\omega_{H_2}/\partial r$, in the vicinity of the cell edge, resulting in the faster molecular average velocity of hydrogen gas than the mass average velocity. On the other hand, the molecular average velocity of the other chemical species including carbon is much slower than that of hydrogen gas. The concentration of the chemical species increases when its velocity decreases because of the continuity law, and the concentration decreases when its velocity increases. The ratio of $H_{balance}/C_{balance}$ then decreases more at r = 56 cm with the lower fuel utilization.

Moreover, for the same fuel utilization, the $H_{balance}/C_{balance}$ is greater as the exit temperature of the pre-reformer is lowered because the non-reformed methane increases, thus resulting in a hydrogen decrease.

As shown above, the experimental result that the ratio of H/C does not remain a constant value in the anode gas for the sealless disk-type SOFC can be explained by a numerical model that considers both the convection and diffusion of the gas.

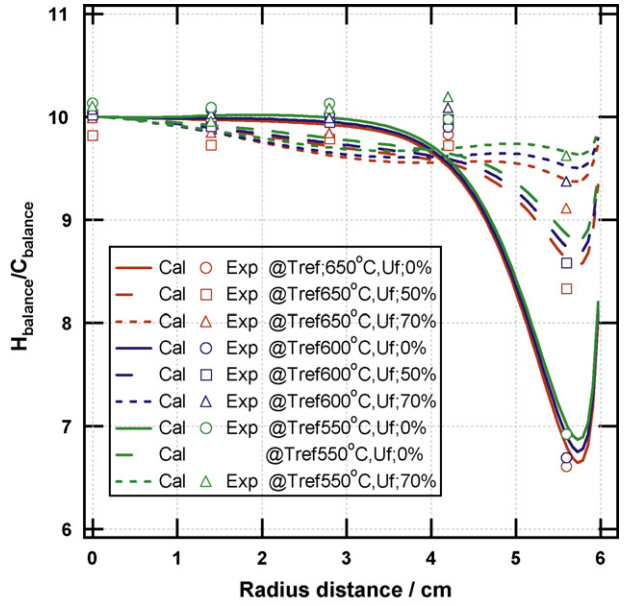

Fig. 16. H/C mass balance.

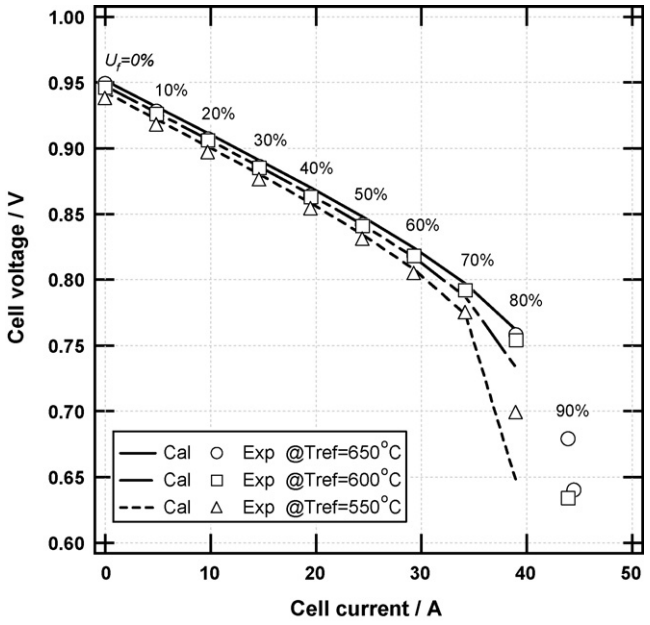

Fig. 17. Voltage–current characteristics.

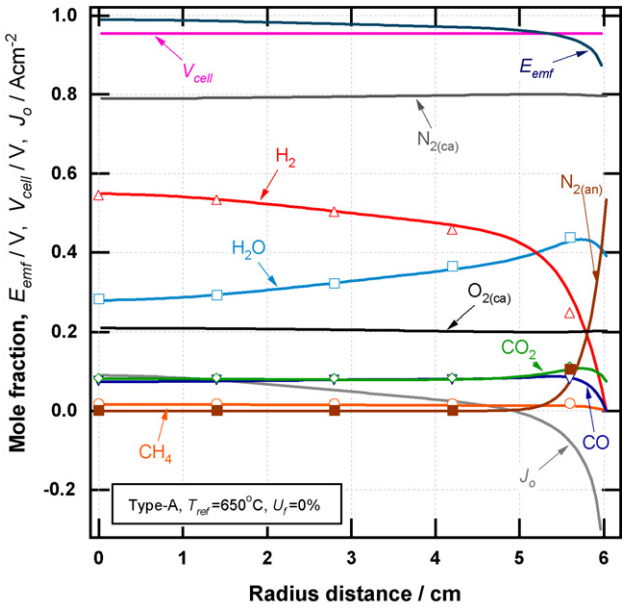

Fig. 18. Distributions of gas concentration, electromotive force, cell voltage, and current density (T_{ref} = 650 °C, U_f = 0%, type-A).

3.1.4. Voltage–current characteristics

Fig. 17 shows a comparison of the voltage–current (V–I) characteristic between the calculation and the experiment results. In the 0–70% range of fuel utilization, the calculated V–I curves are in reasonably good agreement with the experimental plots at each temperature. The validity of the simulation model can also be verified for the cell generating performance characteristic as well as the gaseous chemical reactions. At the fuel utilization of 80%, however, there is the difference from the experimental plots.

Also, it was not possible to calculate up to a 90% fuel utilization by this model at T_{ref} = 650 and 600 °C as mentioned above. One likely reason for this difference is that it relates to the electrolysis current in the vicinity of the outer cell, i.e., it might be not appreciable in this model whether corresponding electrolysis current is obtained between the calculated and experimental results or not, because of writing the each cell resistance by the expression of the simple temperature dependence. Another is that the electrochemical direct reaction of CO might have taken place during the actual reaction, although the reaction is assumed not to in this model. This is also further discussed in Section 3.2. The development of a precise model about these points is future work.

3.2. Anode current collector type-A

Similar to the anode current collector type-C, α_{ref} and α_{sf} are determined by fitting the distributions of the gas concentration at T_{ref} = 600 °C and U_f = 70%. As the sequence for comparison with the experimental data, the following catalytic parameters were obtained; α_{ref} = 0.03 and α_{sf} = 0.005, i.e., ρ_{ref} = 21.2 kg m^{-3} and ρ_{sf} = 3.55 kg m^{-3}. This corresponds to the effective amount of catalyst of 12.7 g m^{-2} for the reforming reaction while that of type-C is 48 g m^{-2}. Although an internal reforming hardly occurs in the type-A during the experiment, it was found that the amount of catalyst per unit area, which contributes to the internal reforming reaction, is almost 1/4 of that for the type-C.

By using these values, the gas concentration distributions are calculated and then compared with the experimental results for each condition when the pre-reformer temperature is 650 and 600 °C and the fuel utilization is 0, 50 and 70%. The distributions of each gas concentration, electromotive force, cell voltage and current density when U_f = 0, 70% as an illustration are displayed in Figs. 18–21. From the figures, for the type-A, the numerical results are also in good agreement with the experimental for every conditions. The results when U_f = 50% are omitted since they also agree well with the experimental data as well as those when U_f = 0, 70%.

When U_f = 70%, it is noted that the calculated CO concentration is higher, while the calculated CO_2 concentration is lower than the experimental data at r = 5.6 cm. It is suggested that the electrochemical direct reaction of CO on the anode might have taken place during the actual reaction because the H_2 concentration is significantly decreasing at $r \geqq 4.2$ cm due to the poor performance of the internal reforming.

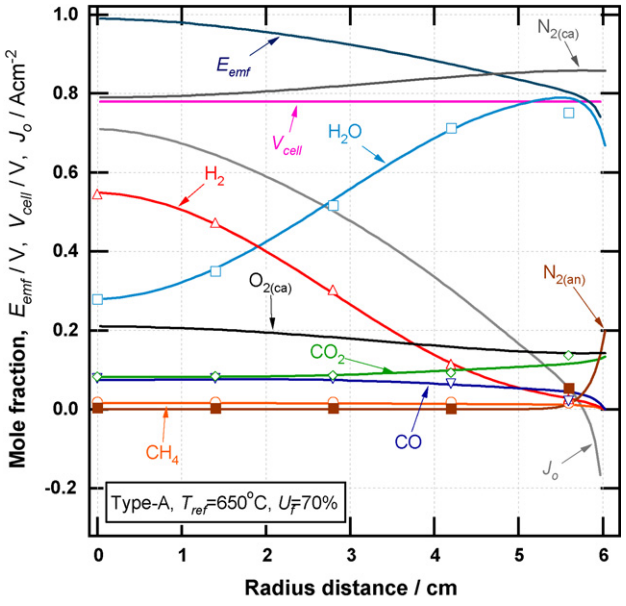

Fig. 19. Distributions of gas concentration, electromotive force, cell voltage, and current density (T_{ref} = 650 °C, U_f = 70%, type-A).

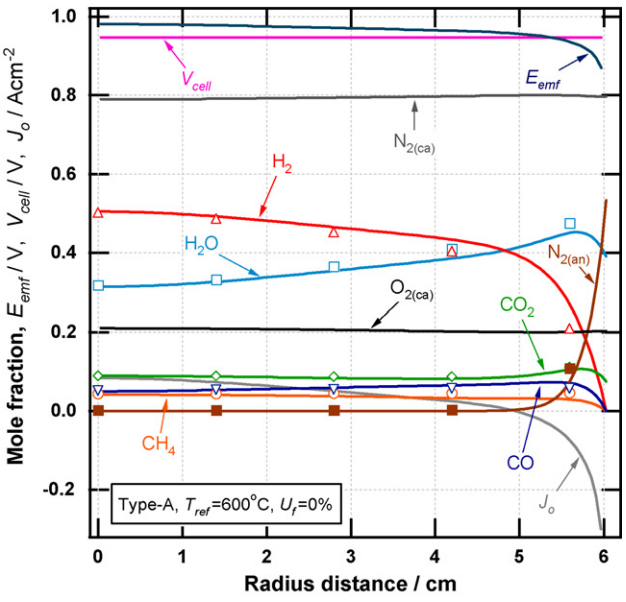

Fig. 20. Distributions of gas concentration, electromotive force, cell voltage, and current density (T_{ref} = 600 °C, U_f = 0%, type-A).

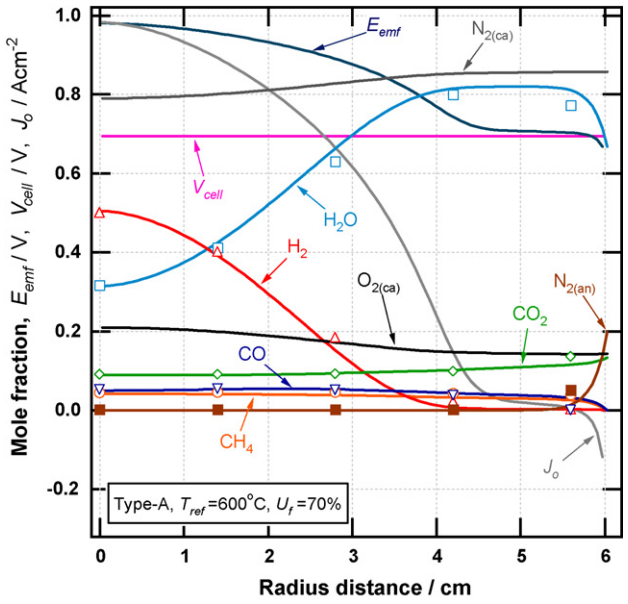

Fig. 21. Distributions of gas concentration, electromotive force, cell voltage, and current density (T_{ref} = 600 °C, U_f = 70%, type-A).

4. Conclusions

The characteristics of the electrical power generation and the internal reforming of a seal-less disk-type SOFC cell have been numerically analysed by a simulation to explain the previously reported experimental results.

From comparisons between the calculations and experimental results for the anode gas concentration profile and the voltage–current characteristics, the validity of the simulation model has been verified, and the model was found to explain the influence of the internal reforming reaction with the water-gas shift reaction, the reverse diffusion of air from the cell circumference and variations in the molar ratio of hydrogen and carbon in the cell outlet region for a disk-type SOFC cell which is operated by partially reformed methane.

Appendix A

Eq. (25) is derived as follows. The equation of mass continuity in the anode is given by

$$\frac{\partial}{\partial t}\rho_{an}\left(\omega_{CH_4}+\omega_{H_2O}+\omega_{H_2}+\omega_{CO}+\omega_{CO_2}+\omega_{N_{2an}}\right)$$
$$+\frac{\partial}{r\partial r}\left[r\rho_{an}\left(\omega_{CH_4}+\omega_{H_2O}+\omega_{H_2}+\omega_{CO}+\omega_{CO_2}+\omega_{N_{2an}}\right)u_{an}\right.$$
$$\left.-r\rho_{an}\left(\begin{array}{l}D_{CH_4m}\dfrac{\partial\omega_{CH_4}}{\partial r}+D_{H_2Om}\dfrac{\partial\omega_{H_2O}}{\partial r}+D_{H_2m}\dfrac{\partial\omega_{H_2}}{\partial r}\\ +D_{COm}\dfrac{\partial\omega_{CO}}{\partial r}+D_{CO_2m}\dfrac{\partial\omega_{CO_2}}{\partial r}+D_{N_{2an}m}\dfrac{\partial\omega_{N_{2an}}}{\partial r}\end{array}\right)\right]$$
$$=\left(\frac{1}{2}\dot{c}_j\right)M_{O_2} \quad (37)$$

The summation of the mass fraction of each gas and that of the mass movement due to mutual diffusion are written as follows:

$$\left(\omega_{CH_4}+\omega_{H_2O}+\omega_{H_2}+\omega_{CO}+\omega_{CO_2}+\omega_{N_{2an}}\right)=1 \quad (38)$$

$$\left(D_{CH_4m}\frac{\partial\omega_{CH_4}}{\partial r}+D_{H_2Om}\frac{\partial\omega_{H_2O}}{\partial r}+D_{H_2m}\frac{\partial\omega_{H_2}}{\partial r}\right.$$
$$\left.+D_{COm}\frac{\partial\omega_{CO}}{\partial r}+D_{CO_2m}\frac{\partial\omega_{CO_2}}{\partial r}+D_{N_{2an}m}\frac{\partial\omega_{N_{2an}}}{\partial r}\right)=0 \quad (39)$$

Therefore, the equation of mass continuity shown as Eq. (25) is obtained, substituting Eqs. (38) and (39) into Eq. (37).

References

[1] F. Nishiwaki, T. Inagaki, J. Kano, J. Akikusa, N. Murakami, K. Hosoi, J. Power Sources 157 (2006) 809–815.
[2] Y. Mizutani, K. Hisada, K. Ukai, H. Sumi, M. Yokoyama, Y. Nakamura, O. Yamamoto, J. Alloys Compd. 408–412 (2006) 518–524.
[3] T. Ono, Y. Ohshima, Y. Hori, T. Shigehisa, A. Kokaji, M. Yoshida, M. Suzuki, T. Sogi, K. Higaki, A. Chikazawa, Fuel Cell Seminar Abstracts (2006) 144–147, 2006.
[4] S.D. Mehta, R.P. Danner, Ind. Eng. Chem. Fundam. 24 (1985) 325–330.
[5] E. Achenbach, J. Power Sources 49 (1994) 333–348.
[6] M. Bistolfi, A. Malandrino, N. Mancini, Comput. Chem. Eng. 20 (1996) S1487–S1491.
[7] M. Iwata, T. Hikosaka, M. Morita, T. Iwanami, K. Ito, K. Onda, Y. Esaki, Y. Sakaki, S. Nagata, Solid State Ionics 132 (2000) 297–308.
[8] S. Nagata, A. Momma, T. Kato, Y. Kasuga, J. Power Sources 101 (2001) 60–71.
[9] P. Aguiar, D. Chadwick, L. Kershenbaum, Chem. Eng. Sci. 57 (2002) 1665–1677.
[10] K.P. Recknagle, R.E. Williford, L.A. Chick, D.R. Rector, M.A. Khaleel, J. Power Sources 113 (2003) 109–114.
[11] T. Ota, M. Koyama, C. Wen, K. Yamada, H. Takahashi, J. Power Sources 118 (2003) 430–439.
[12] L. Petruzzi, S. Cocchi, F. Fineschi, J. Power Sources 118 (2003) 96–107.
[13] A.C. Burt, I.B. Celik, R.S. Gemmen, A.V. Smirnov, J. Power Sources 126 (2004) 76–87.
[14] N. Autissier, D. Larrain, J. Van herle, D. Favrat, J. Power Sources 131 (2004) 313–319.
[15] B.A. Haberman, J.B. Young, Int. J. Heat Mass Transfer 47 (2004) 3617–3629.
[16] H. Yakabe, T. Sakurai, Solid State Ionics 174 (2004) 295–302.
[17] A. Momma, Y. Kaga, K. Takano, K. Nozaki, A. Negishi, K. Kato, T. Kato, T. Inagaki, H. Yoshida, K. Hoshino, M. Yamada, T. Akbay, J. Akikusa, J. Power Sources 145 (2005) 169–177.
[18] W. Jiang, R. Fang, J.A. Khan, R.A. Dougal, J. Power Sources 162 (2006) 316–326.
[19] J.-M. Klein, Y. Bultel, S. Georges, M. Pons, Chem. Eng. Sci. 62 (2007) 1636–1649.
[20] A. Momma, K. Takano, Y. Tanaka, A. Negishi, K. Kato, M. Amano, K. Nozaki, T. Kato, T. Inagaki, M. Kawano, K. Hosoi, K. Hoshino, M. Shibata, T. Akbay, J. Akikusa, N. Chitose, in: K. Eguchi, S.C. Singhal, H. Yokokawa, J. Mizusaki (Eds.), Solid Oxide Fuel Cells 10, ECS Trans. 7 (2007) 805–814.
[21] R. Odegard, E. Johnsen, H. Karoliussen, Proc. Solid Oxide Fuel Cell IV (1995) 810–819.
[22] A.L. Lee, R.F. Zabransky, W.J. Huber, Ind. Eng. Chem. 29 (1990) 766–773.
[23] R.L. Keiski, T. Salmi, P. Niemisto, J. Ainassaari, V.J. Pohjala, Appl. Catal. A 137 (1996) 349–370.
[24] D.F. Fairbanks, C.R. Wilke, Ind. Eng. Chem. 42 (1950) 471–475.
[25] R.C. Reid, J.M. Pravsnitz, T.K. Sherwood, The Properties of Gases and Liquids, third ed., McGraw-Hill, 1977.
[26] Y. Takeuchi (Ed.), Porous Materials—Characterization, Production and Application, FUJI Techno System, 1999, pp. 336.